



### **Science Arts & Métiers (SAM)**

is an open access repository that collects the work of Arts et Métiers Institute of Technology researchers and makes it freely available over the web where possible.

This is an author-deposited version published in: <https://sam.ensam.eu>  
Handle ID: [.http://hdl.handle.net/10985/24790](http://hdl.handle.net/10985/24790)

#### **To cite this version :**


Sevan GAROIS, Monzer DAOUD, Khalil TRAIKI, Francisco CHINESTA SORIA - Artificial intelligence modeling of induction contour hardening of 300M steel bar and C45 steel spur-gear - International Journal of Material Forming - Vol. 16, n°3, - 2023

Any correspondence concerning this service should be sent to the repository

Administrator : [scienceouverte@ensam.eu](mailto:scienceouverte@ensam.eu)



# Artificial intelligence modeling of induction contour hardening of 300M steel bar and C45 steel spur-gear

Sevan Garois<sup>1</sup>  · Monzer Daoud<sup>2</sup> · Khalil Traidi<sup>3</sup> · Francisco Chinesta<sup>1</sup>

Received: 24 October 2022 / Accepted: 27 February 2023

© The Author(s), under exclusive licence to Springer-Verlag France SAS, part of Springer Nature 2023

## Abstract

Induction hardening is a heat surface treatment technique widely employed for steel components in order to improve their fatigue life without affecting the metallurgy of the bulk material. The control of the treated components goes through the prediction and the optimization of the induction hardening process parameters. The aim of this work is to propose an approach based on artificial intelligence technique to predict the in-depth hardness profile. For this purpose, experimental tests were first carried out on 300M steel bar and C45 steel spur-gear under single and double frequencies, respectively. Intermediate variables were then generated to be used as input data. Data-driven model based on XGBoost library was finally developed. It was found that the proposed approach predicts with good agreement the hardness profiles and can be used in induction treatment process optimization.

**Keywords** Induction hardening · Hardness · Artificial intelligence technique · Data-driven model · XGBoost

## Introduction

Induction hardening is a multi-physics process which is widely employed to enhance the fatigue behavior of many critically loaded mechanical workpieces in automotive and aerospace industries. During the process, the ferrous components such as steel grades are rapidly heated to a very high temperature (heating phase), then quickly cooled to room temperature (quenching phase) [1]. As a result, a fine-grain martensite phase [2, 3] as well as a compressive residual stress field [4] are induced in the superficial layer which

enhance fatigue life of engineering components [5, 6]. Industries use more and more this process because it provides a high quality over time, good repeatability, fast, and clean processing for precise heating of the interested zones without affecting the metallurgy of the bulk material. [7, 8].

The main process parameters are the frequency, power level of the employed source currents, and heating time. Depending on how the frequency is applied, there are two usual heating approaches that can impact the heating phase. The former is induction with a single-frequency and the latter one consists of combining two different frequencies, medium and high frequencies, applied simultaneously or sequentially. These two approaches have been employed in numerical and experimental investigations. It is worth mentioning that these two approaches have differences in terms of precision and quality of the treatment [9]. In fact, the use of a double-frequency induction heating allows a full hardening of the superficial layer of a complex geometry, which can be incomplete with the single-frequency heating [10].

In practical applications, an appropriate selection of the process parameters is highly important to carry out a desired contour free of cracks. Many experimental investigations have been carried out to study this induction surface hardening process. These investigations have focused on the influence of process parameters on the induced residual stresses of hardened cylindrical specimens [11], the

---

✉ Sevan Garois  
sevan.garois@ensam.eu

Monzer Daoud  
monzer.daoud@irt-m2p.fr

Khalil Traidi  
khalil.traidi@safrangroup.com

Francisco Chinesta  
francisco.chinesta@ensam.eu

<sup>1</sup> PIMM Laboratory, Arts et Métiers Institute of Technology, CNRS, Cnam, HESAM Université, 151 Boulevard de l'Hôpital, 75013 Paris, France

<sup>2</sup> Institut de Recherche Technologique Métallurgie Matériaux et Procédé, 4 Rue Augustin Fresnel, 57070 Metz, France

<sup>3</sup> Safran Tech, Rue des Jeunes Bois, 78117 Châteaufort, France

relationship between the change in mechanical properties and the microstructure of 45 steel bars [12], the effects of different quenching parameters on distortion of cylindrical parts [13], the influence of different grinding parameters on residual stress results [14], the effects of spray cooling for gearwheel induction [15], the consequences of the variation of initial hardness level of discs on the distortion and hardening depth [16]. However, experimental approach is not only time consuming but requires significant experimental tests for a restricted validation range. More promising approach for orienting and optimizing the experimental activity is provided by numerical techniques such as the finite element method (FEM). It has proven to be highly efficient for dealing with multiphysics-based parametrized problems thanks to the advanced numerical simulation codes [17]. Consequently, a large number of research works has focused on the use of FEM to analyze the hardness [18, 19], the temperature field [20, 21], the residual stress fields [22] and the microstructure [19, 23].

Although the different mechanical and microstructural fields are predicted, 3D-FEM still suffers from some drawbacks. To name a few, they are high computational cost, supporting the use of multiple frequencies, and data exchange between solvers [24, 25].

Several analytical models have been proposed and used mainly to describe the phenomena involved during the induction hardening process [26–30]. However, these models are very limited by the geometry of the inductor and the workpiece. This made way to integrate analytical models to the FEM to solve the coupled electromagnetic-thermomechanical problem [31, 32]. The computational time, however, is still too high.

In recent years, the rise of different machine learning algorithms, coupled with more efficient optimization techniques, allows a relevant alternative for this type of analyses [33–35]. Machine learning represents different techniques such as Artificial Neural Network (ANN), Random Forest (RF) or Gradient-Boosted Trees (GBT). The classical machine learning pipeline (sequence of actions) for modeling is used to analyze the data, treat the variables, split them into train and test sets, fit and construct the model, predict the results with testing data, and compare the model predictions with the ground truth to quantify the result error. ANN are regularly involved in metallurgy analysis under induction heating [36], surface hardness in carburizing quenching [37] and in laser hardening [38], and various mechanical properties in metal rolling [39]. Also, machine learning algorithms from the XGBoost library [40] are recognized of being efficient in some challenges while being convenient in the use and optimization [41]. Despite the relative well-known lack of data in the field of metallurgy, it is possible to propose reliable models. In fact, XGBoost has been used with success for predicting some mechanical properties like hardenability

[42] and tensile strength, compressive strength, and elongation of hot-rolled strips [43] using small and big datasets, respectively.

The literature review shows a particular interest on both single and double-frequency induction hardening experiments [44] either to validate results obtained by modeling in FEM [45] or to optimize the process parameters [46]. Studying both of them should be interesting anyway.

This work aims at proposing an approach based on artificial intelligence technique to build more predictive fast running models of the induced hardness profile within a cylindrical bar of 300M steel alloy and spur-gear of C45 steel during the induction heating process. To conduct such a study, experimental data under single and double frequencies are presented in Section 2. Section 3 concerns the development of data-driven model based on XGBoost library to predict the hardness profile under the effect of the process parameters. The obtained results are presented and discussed in Section 4. The main conclusions and the relevancy of the work are exposed in Section 5.

## Experimental procedure

### Induction hardening of cylindrical bars

The first series of experiments were conducted on a cylindrical bar made of 300M low alloy steel. The process parameters are listed in Table 1. During these experiments, samples rotated around a vertical axis and each one was used to carry out several induction treatments at different positions sufficiently spaced to avoid any eventual interaction effects which was verified by the infrared camera. The heating phase was carried out by a ring inductor encircling the sample and having

**Table 1** Induction heat treatment conditions for cylindrical samples

Run #	Frequency $F$ (kHz)	Power $P$ (kW)	Time $t$ (s)	Temperature $T$ (°C)
1	224	33	0,15	892
2	224	33	0,2	958
3	224	33	0,3	1008
4	224	33	0,85	1121
5	224	33	1,3	1265
6	224	19	1	927
7	224	19	3,0	1034
8	224	19	3,5	1134
9	224	19	4,5	1277
10	224	49	0,15	1025
11	224	49	0,2	1142
12	224	49	0,08	1085

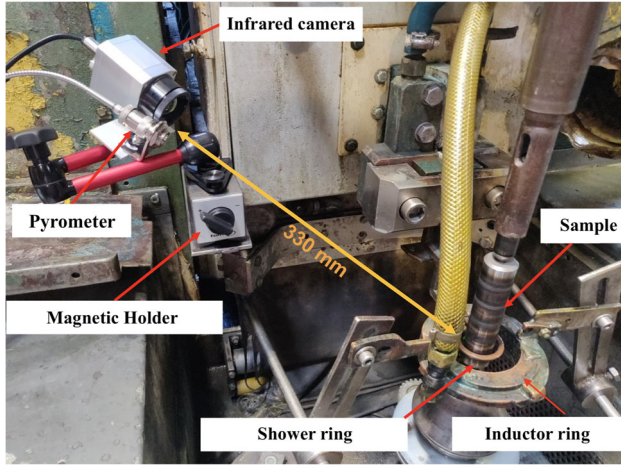


**Fig. 1** Experimental setup utilized during the induction hardening treatment of cylindrical bars under a high single-frequency

a rectangular shape of 2x5mm and an air-gap of 3mm while the subsequent cooling shower of a polymer-water mixture was applied by another coaxial ring as shown in Fig. 1. During heating, temperature measurements on surface were obtained using a bichromatic pyrometer (see Table 1) while the in-depth temperature profile was predicted based on FEM (see Fig. 2). Micro-hardness Vickers (HV0.3) profiles were carried out in the radial direction of the sample in order to determine the penetration hardening. These analyses were performed after the induction treatment and performed on a transversal section according to ISO 6507 [47].

### Induction hardening of gears

The second series of experiments were carried out on C45 steel spur gears. The main gear data were summarized in Table 2 while the process parameters were listed in

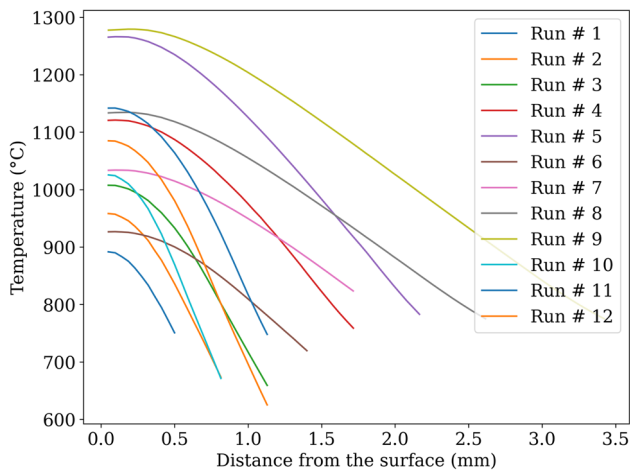


**Fig. 2** Predicted in-depth temperature profiles by FEM for experimental runs

Tables 3 and 4. For these experiments, gears were mounted on a rotating chuck during the process. An Optris pyrometer was used to measure the temperature on surface at the tooth root during the treatment. The heating phase was conducted with ring inductor encircling the sample having a rectangular shape of 12.25x20mm and an air-gap of 2mm while the subsequent cooling shower of a polymer-water mixture was applied by another coaxial ring as shown in Figure 3. Micro-hardness Vickers (HV0.3) profiles were carried out in the radial direction of the sample at the tooth tip and the tooth root in order to determine the penetration hardening on these two locations. These analyses were performed after the induction treatment and performed on a transversal section according to ISO 6507 [47].

It is worth noting that the frequency ranges from 12 to 14 kHz in MF and from 150 to 350 kHz in HF. The final measured frequency depends on the torque between the gear and the inductor. So, the measured frequency will not be the same, especially in high frequency. It is clear that the frequencies are not the main variable to describe the system due to their slight variation. This point will be investigated in next sections.

## Hardness modeling

### XGBoost algorithm

In the present work, the EXtrem Gradient Boosting (XGBoost) algorithm was chosen because it is one of the most effective boosting tree algorithms for gradient boosting machine (GBM) and highly efficient for machine learning prediction problems with a few pre-processing requirements [48, 49]. It has the advantage of being convenient and easy to test and manipulate because there is no need to search and optimize an architecture like neural networks: only a few hyperparameters related to the trees such as the maximum depth or the number of estimators. Moreover, it has been proven that the XGBoost is robust enough [50, 51] while requiring a satisfying training time. XGBoost is based on gradient-boosted decision-tree. In fact, XGBoost build sequentially a forest of gradient boosted decision trees. For the sake of completeness here we briefly revisit the technique, and for a deeper illustration, the interested reader can refer to Appendix A.

Each iteration of a tree compute the residuals  $r_k$  of each  $k$  observed value  $y_{obs,k}$  of the dataset with respect to a predicted value  $y_{pred,k}$ :

$$r_k = y_{obs,k} - y_{pred,k} \quad (1)$$

The residuals are collected in the first leaf of the tree called the root node. The goal is to split considering a threshold condition on a given variable. Each possible split is defined

**Table 2** Gear data for double-frequency induction hardening experiments

Gear #	Module	No. of teeth	Width	Addendum circle	Pitch circle	Root circle
1	2.5	22	10 mm	60 mm	55 mm	48.75 mm
2	3	18	10 mm	60 mm	54 mm	46.5 mm

by the average value between two consecutive observed data points. The residuals are used to compute the similarity score  $S$ , which is defined as

$$S = \frac{(\sum_{k=1}^m r_k)^2}{m + \lambda} \quad (2)$$

where  $m$  is the number of residuals and  $\lambda$  is the user-defined regulation hyperparameter. Depending on the value of  $S$ , the

different residuals are set into the right and left leaves given the chosen split, making new similarity scores. In fact,  $S$  score of the root node and the left and right leaves are used to calculate the gain  $G$  such as:

$$G = S_{left} - S_{right} - S_{root} \quad (3)$$

The split inducing the highest gain  $G$  is kept. Then, splits can be made again on the lastest nodes. A branch with a negative

**Table 3** Induction heat treatment conditions for gears with module  $m=2.5$ 

Run #	Medium Frequency $MF$ (kHz)	High Frequency $HF$ (kHz)	Power of $HF$ $P_{HF}$ (kW)	Power of $MF$ $P_{MF}$ (kW)	Time $t$ (s)	Temperature $T$ (°C)
1	13	256	143	88	0,17	780
2	12	258	225	138	0,17	1080
3	12	258	225	138	0,2	1200
4	12	257	143	113	0,17	835
5	12	258	184	113	0,17	935
6	12	258	225	113	0,17	1005
7	13	257	143	113	0,2	×
8	13	257	184	88	0,2	917
9	13	257	184	138	0,24	1189
10	13	257	143	138	0,2	1059
11	12	257	184	113	0,2	1025
12	13	257	184	88	0,24	1028
13	12	258	225	88	0,2	999
14	13	257	143	88	0,24	925
15	12	258	225	113	0,24	1167
16	12	258	225	88	0,17	900
17	12	257	184	138	0,17	1005
18	13	257	143	113	0,24	1039
19	13	257	143	138	0,24	1145
20	12	258	225	138	0,24	1217
21	12	258	225	88	0,18	884
22	12	258	198	134	0,17	920
23	×	×	238,5	94	0,17	890
24	×	×	247,5	98	0,19	958
25	12	257	202	110	0,17	884
26	×	×	175,5	102	0,19	889
27	12	257	202,5	118	0,17	887
28	×	×	193,5	102	0,19	876
29	×	×	238,5	88	0,19	906
30	×	×	247,5	88	0,19	905
31	×	×	247,5	94	0,17	858

×: missing values

**Table 4** Induction heat treatment conditions for gears with module  $m=3$ 

Run #	Medium Frequency $MF$ (kHz)	High Frequency $HF$ (kHz)	Power of $HF$ $P_{HF}$ (kW)	Power of $MF$ $P_{MF}$ (kW)	Time $t$ (s)	Temperature $T$ (°C)
1	12	254	143	88	0,17	800
2	12	256	225	138	0,17	1100
3	12	255	225	138	0,2	×
4	12	254	143	113	0,17	×
5	12	255	184	113	0,17	969
6	12	256	225	113	0,17	992
7	13	254	143	113	0,2	982
8	12	255	184	88	0,2	909
9	13	255	184	138	0,24	1166
10	12	254	143	138	0,2	1075
11	12	255	184	113	0,2	1040
12	12	255	184	88	0,24	1025
13	12	255	225	88	0,2	1025
14	12	254	143	88	0,24	959
15	12	255	225	113	0,24	1197
16	12	256	225	88	0,17	970
17	12	255	184	138	0,17	1045
18	12	254	143	113	0,24	1030
19	12	254	143	138	0,24	1135
20	12	256	225	138	0,24	1293

gain should be removed as the tree is pruned. The output value of the full tree is expressed as:

$$y_{output} = \frac{\sum_{k=1}^m r_k}{(m + \lambda)} \quad (4)$$

The predicted value of the tree  $\hat{y}_n$  using the previous one  $\hat{y}_{n-1}$  and the output  $y_{output}$  of the built tree is obtained as

follows:

$$\hat{y}_n = \hat{y}_{n-1} + \eta \cdot y_{output} \quad (5)$$

where  $\eta$  is the learning rate. If  $n = 1$ ,  $y_0$  is a default value. Now a single tree is built and the predicted values  $\hat{y}_n$  are involved for the calculation of the residuals of the next tree. The goal is to minimize the residuals to a value close to 0. When all trees are built it is possible to compute a final and accurate prediction  $\hat{y}$ , it is defined as a weighted sum of trees output and can be written as:

$$\forall i \in [1; n], \hat{y} = \sum_{i=1}^n \eta \cdot y_{output,i} \quad (6)$$

where  $n$  is the final number of trees. The final ensemble of trees can be summarized in Fig. 4.

### Extraction of intermediate parameters

Extraction of intermediate parameters of any system for the training phase is highly important. This is because, in the present work, the temperature profiles and the surface temperature for cylindrical bars and gears, respectively, were considered as an important parameter to describe the hardness. In fact, preliminary analysis have shown that first results

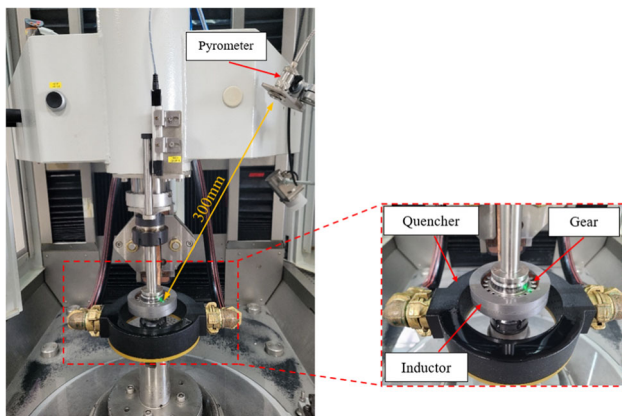
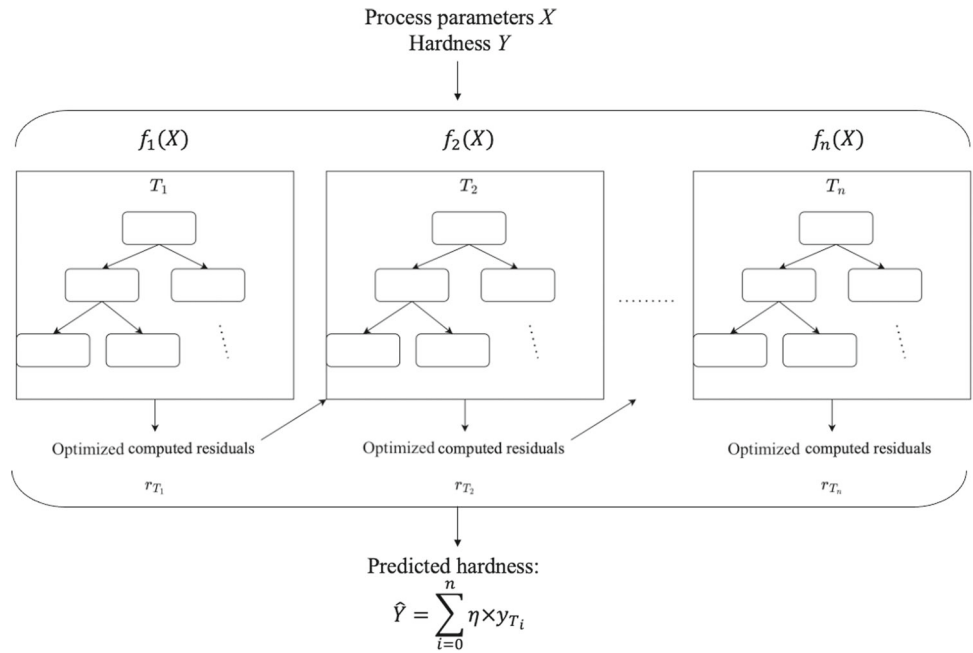


**Fig. 3** Experimental setup utilized during the induction hardening treatment of gears under a double-frequency

**Fig. 4** Ensemble of the XGBoost trees



lacked of accuracy without it. The temperature is not a machine parameter and requires a particular system (pyrometer or thermocouple) to be measured which is not present in the industrial case. Therefore, the temperature was predicted to be used as input for hardness modeling. Predictions were carried out using XGBoost algorithm using the process parameters previously listed in Table 3 as input without any further optimization. Figures 5 and 6 show the comparison between the real and the predicted heating temperature for cylindrical bars and gears, respectively. The test error for both

predictions was found to be 1.5% and 0.24%, for cylindrical bars and gears, respectively. These results indicated that the XGBoost algorithm gave a good prediction of the heating temperature.

### Determination of space of variables for different cases

In order to use all the collected data with some missing ones, it is necessary to consider several cases.

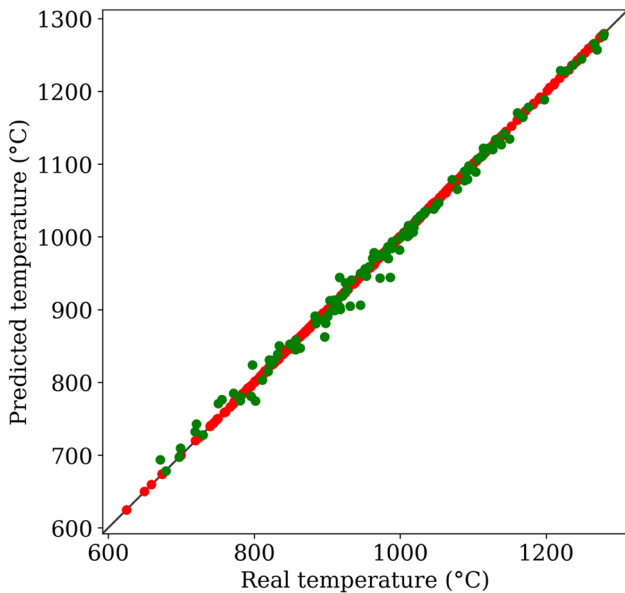


**Fig. 5** Predicted versus real in-depth temperatures for cylindrical bars showing training (red) and testing (green) data points

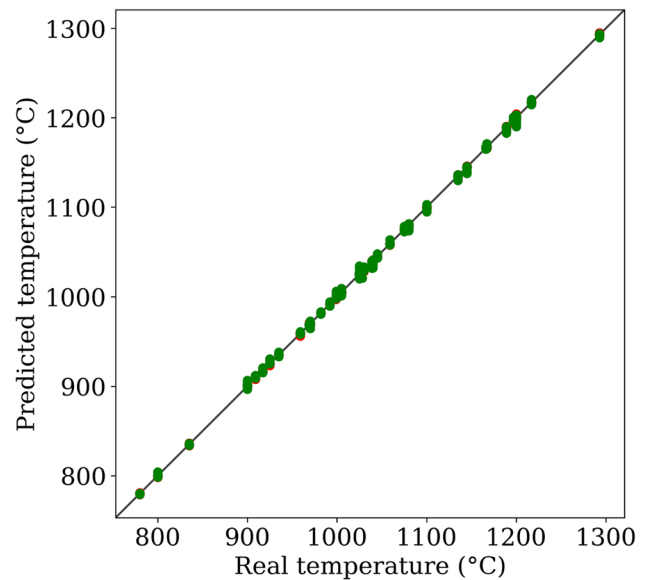


**Fig. 6** Predicted versus real surface temperatures for gears showing training (red) and testing (green) data points

## Experiments carried out on cylindrical bars

The space of variables for the induction hardening of cylindrical bars is expressed as:

$$X_{1f} = F, P, T, d, t \quad (7)$$

where  $F$  is the frequency;  $P$  is the generator power;  $T$  is the in-depth temperature;  $d$  is the depth at which the hardness was measured and  $t$  is the heating duration.

## Experiments carried out on gears

In general, the space of variables for the induction hardening of gears could be expressed as:

$$X_{2f} = \{MF, HF, P_{MF}, P_{HF}, T, d, t\} \quad (8)$$

where  $MF$  and  $HF$  are the medium and high frequency respectively;  $P_{MF}$  and  $P_{HF}$  are their respective generator powers;  $T$  is the temperature measured at the side surface close to the tooth root;  $d$  is the depth at which the hardness was measured, and  $t$  is the heating duration.

*Case 1: Cloud of points-based dataset from both modules*

The space of variables could be expressed as:

$$X_{C1} = \{MF, HF, P_{MF}, P_{HF}, T, t, d\} \quad (9)$$

The dataset is composed of two subsets of 20 runs each for each gear module. In this first case, the two subsets are merged to make a greater dataset allowing to verify if there is a significant difference of the hardness measured between the two gear modules data. This dataset contains a total of 2215 randomly mixed data points. Usually, and in the rest of this work, 70% of the dataset is considered for training, leaving 30% to the testing phase. Here, it represents 1697 training points versus 518 testing points

*Case 2: Cloud of points-based dataset added from module 2.5 gear*

The second case brings new data concerning the gear with module 2.5 with 4 extra runs added to the initial induction heat treatment conditions. The space of variables remains as case 1:

$$X_{C2} = \{MF, HF, P_{MF}, P_{HF}, T, t, d\} \quad (10)$$

In this case, 1058 points were considered for training, leaving 322 to the testing phase.

*Case 3: Cloud of points-based dataset with frequencies taken off*

In this case, the modeling was carried out without frequencies and hence the space of variables is given as:

$$X_{C3} = \{P_{MF}, P_{HF}, T, t, d\} \quad (11)$$

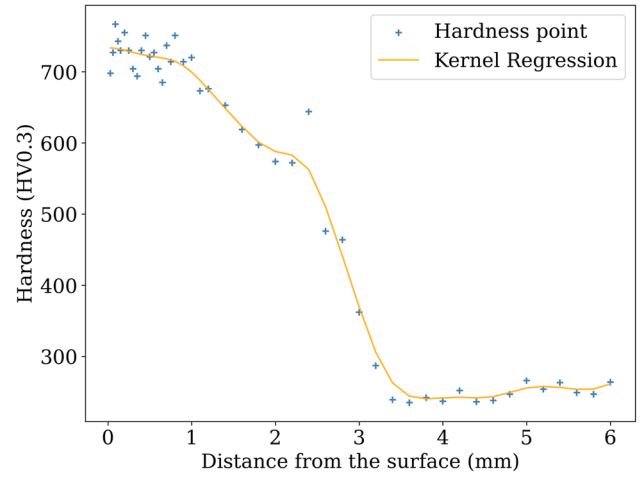


Fig. 7 Smoothed in-depth hardness profile using Kernel regression

In this case, 1426 points were considered for training, leaving 434 to the testing phase.

*Case 4: Profiles-based dataset without frequencies*

In this case, data points were aggregated into profiles with respect to their run. Therefore, 24 profiles were considered for training, leaving 7 profiles to the testing phase.

## Data smoothing and experimental variation area

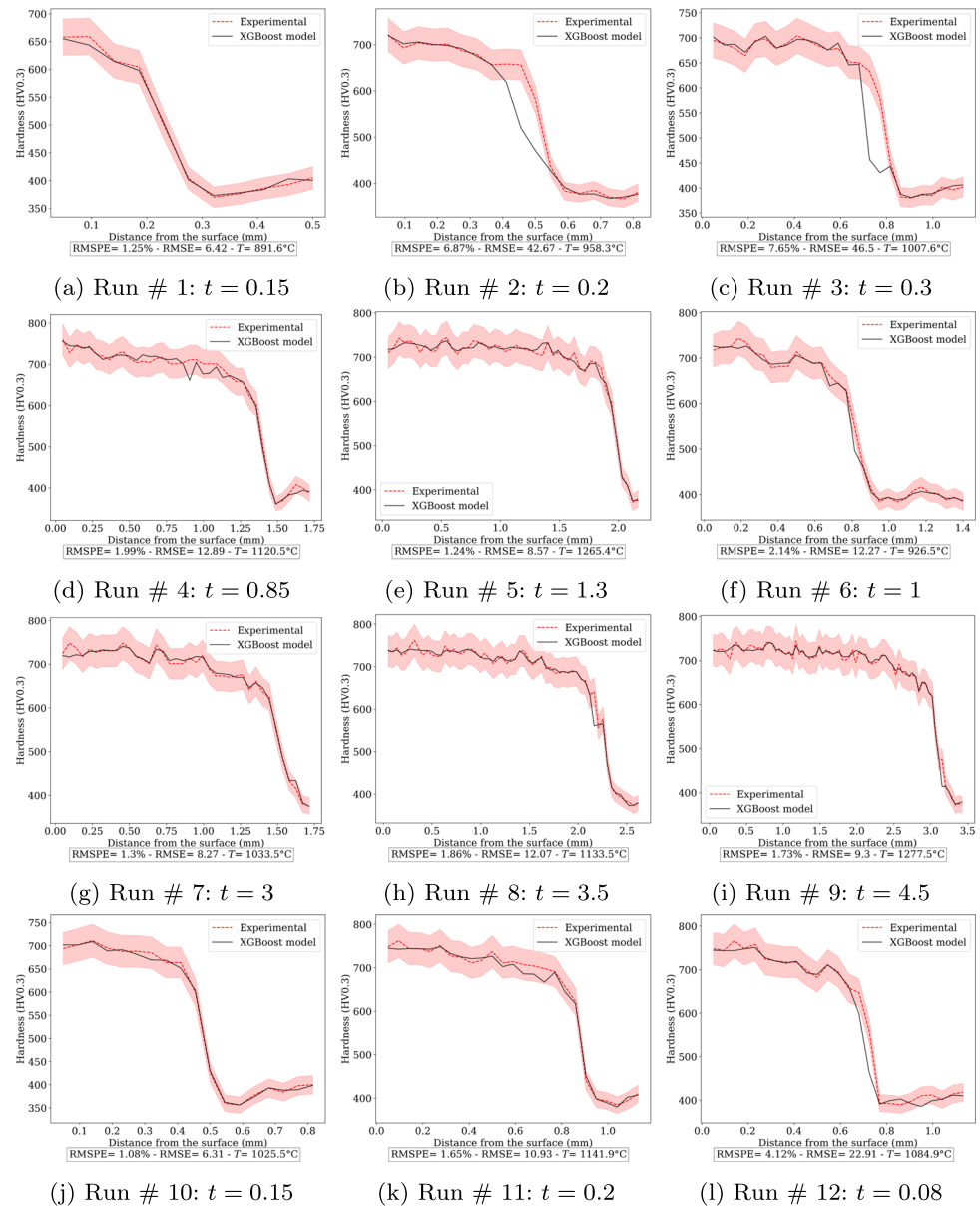
Experimental data are noisy because of the intrinsic physical variability and the uncertainty of measurements. Therefore, it is interesting to smooth the data to increase model training ease. The data to be smoothed are the hardness profiles. There are several statistical methods for reducing output noise. For this work, the method of Kernel Regression [52] was chosen because it implies a conditional expectation. Figure 7 shows the smoothed in-depth hardness profile.

Moreover, after applying Kernel Regression to smooth the data, the noisy nature of the data was taken into account by integrating an experimental variation area. Each smoothed point has a higher and lower hardness point defining the experimental variation area. This area was considered up to  $\pm 5\%$  of the smoothed hardness as set by industrial practice and will be illustrated in the next Figures as a light-red zone.

Table 5 XGBoost and Random Forest results for hardness prediction for cylindrical bars

Model	XGBoost	Random Forest
$RMSE_{train}$	5.57	11.14
$RMSE_{test}$	28.64	32.73
$RMSP E_{train}$	<b>0.93%</b>	<b>2.17%</b>
$RMSP E_{test}$	<b>5.42%</b>	<b>6.37%</b>

**Fig. 8** Comparison of the XGBoost model with the experimental hardness for the cylindrical bars treated under single frequency.  $T$  represents the measured surface temperature



## Optimized data selection

Specifically for the case 4, because each run belongs to only one set, either train or test, the number of different values for each variable is restricted in each. Hence, the train test split stage has particularly a large impact on the final result because all patterns are not necessarily represented in the training set. To have the most suitable patterns in the training set, a selection is made for the training set based on the test results so the predictions could be more accurate. This allows

to avoid extrapolation and to take data that are more likely to train the model.

## Results and discussion

### Hardness profile prediction in the cylindrical bar

A Random Forest (RF) regressor as well as the XGBoost model were used for a comparative investigation. The

metrics used to evaluate the results are the Root Mean Squared Error (RMSE) and the Root Mean Squared Percentage Error (RMSPE) which is a relative error. They are defined as follows in Eq. 12.

$$RMSE = \sqrt{\frac{1}{n} \sum_{i=1}^n (y_{pred} - y_{true})^2}$$

$$RMSPE = \sqrt{\frac{1}{n} \sum_{i=1}^n \left(\frac{y_{pred} - y_{true}}{y_{true}}\right)^2} \times 100 \quad (12)$$

where  $y_{true}$  and  $y_{pred}$  are the real hardness and the predicted one, respectively. As can be seen in Table 5, although the RF shows good results, the XGBoost gives better prediction with smaller relative errors. It is worth mentioning that even though this problem involves complex multi-physical behavior, the geometry being a simple cylinder makes it relatively easy to treat. Hence, it is clear that the results are good enough and that the RF could be considered as an alternative approach.

Figure 8 shows the predicted and experimental in-depth hardness profiles. As shown in this figure, three zones could be identified from the surface: a hardened zone, a transition zone where the hardness drops drastically, and the core of the workpiece unaffected by the induction treatment. Although the predicted profile exceeds the experimental variation area at certain zones, it appeared that the predicted profiles gave the same trends and the same type of hardness level at surface as the measured ones.

### Hardness profile prediction in the gear

All the errors obtained after modeling each of the different cases presented in Section 3 are analyzed and listed in Table 6. Firstly, for each cases the tooth tip seems to be easier to predict than the tooth root. This could be explained by the fact that there is comparatively more data in the tooth tip. However, it is noticeable that this tendency is reversed in the case of indivisible profiles. This could be explained by the fact that the profiles in the tooth are comparatively less diverse than in the tooth tip.

Secondly, it is interesting to see that whatever the case studied: different modules, different frequencies and powers, with or without frequency and profile-based dataset, the results remain more or less always precise. Therefore, there is a certain global efficiency to describe different cases for a global overview, despite some differences in the inputs.

In any case, the error being always lower than 10%, it is reasonable to say that the numerical results are encouraging and satisfying.

**Table 6** Training and testing errors of the XGBoost models at the tooth tip and the tooth root for different cases

Case #	XGBoost Error	Tooth root	Tooth tip
1	$RMSE_{train}$	5.75	3.13
	$RMSE_{test}$	24.43	17.92
	$RMSP E_{train}$	<b>1.37%</b>	<b>0.80%</b>
	$RMSP E_{test}$	<b>6.93%</b>	<b>4.73%</b>
2	$RMSE_{train}$	7.53	2.4
	$RMSE_{test}$	24.75	19.27
	$RMSP E_{train}$	<b>1.90%</b>	<b>0.57%</b>
	$RMSP E_{test}$	<b>6.44%</b>	<b>4.58%</b>
3	$RMSE_{train}$	7.97	3.21
	$RMSE_{test}$	28.90	18.73
	$RMSP E_{train}$	<b>2.02%</b>	<b>0.78%</b>
	$RMSP E_{test}$	<b>8.21%</b>	<b>4.84%</b>
4	$RMSE_{train}$	0.52	2.26
	$RMSE_{test}$	28.22	35.46
	$RMSP E_{train}$	<b>0.1%</b>	<b>0.54%</b>
	$RMSP E_{test}$	<b>6.07%</b>	<b>8.2%</b>

For the sake of clarity, only few results were presented in Figs. 9, 10 and 11. Nonetheless, more testing runs of the case 4 will be displayed because it is considered as a validation case. Finally, it is worth mentioning that data from gear with module 3 are not modeled after case 1 because the results obtained in that case prove that it is possible with the data merged from both of these gears to have a relevant hardness prediction. Moreover, data from gear with module 2.5 has more and complete available data. Therefore, it was chosen for further modeling.

It is clear that for each case, regardless of the illustrated run, The XGBoost predictions were in good agreement with the experimental results.

Although some errors appear more remarkable than in the previous cases, as in Fig. 12(b), the XGBoost results are still in good agreement with the experimental hardness profiles and none of them is inconsistent. This case serving as a global validation of the ability of an XGBoost model to describe the hardness of an hardened gear, the model presented is quite efficient and accurate.

### Conclusion

In this work, an approach based on artificial intelligence technique was developed to predict the in-depth hardness profile

**Fig. 9** Comparison of the XGBoost model with the experimental hardness for the gear treated under double frequency - Case 1.  $T$  is the measured surface temperature

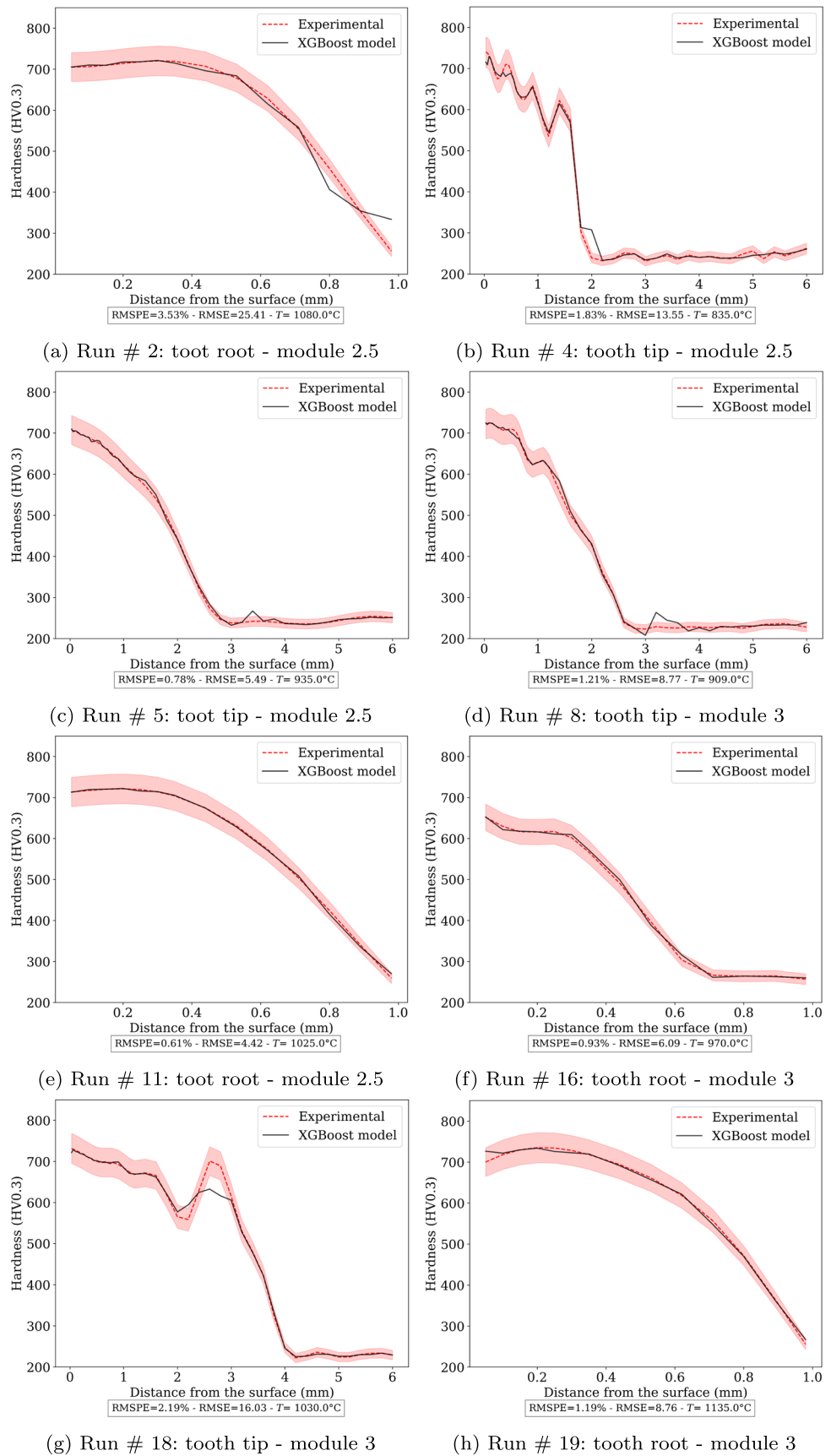
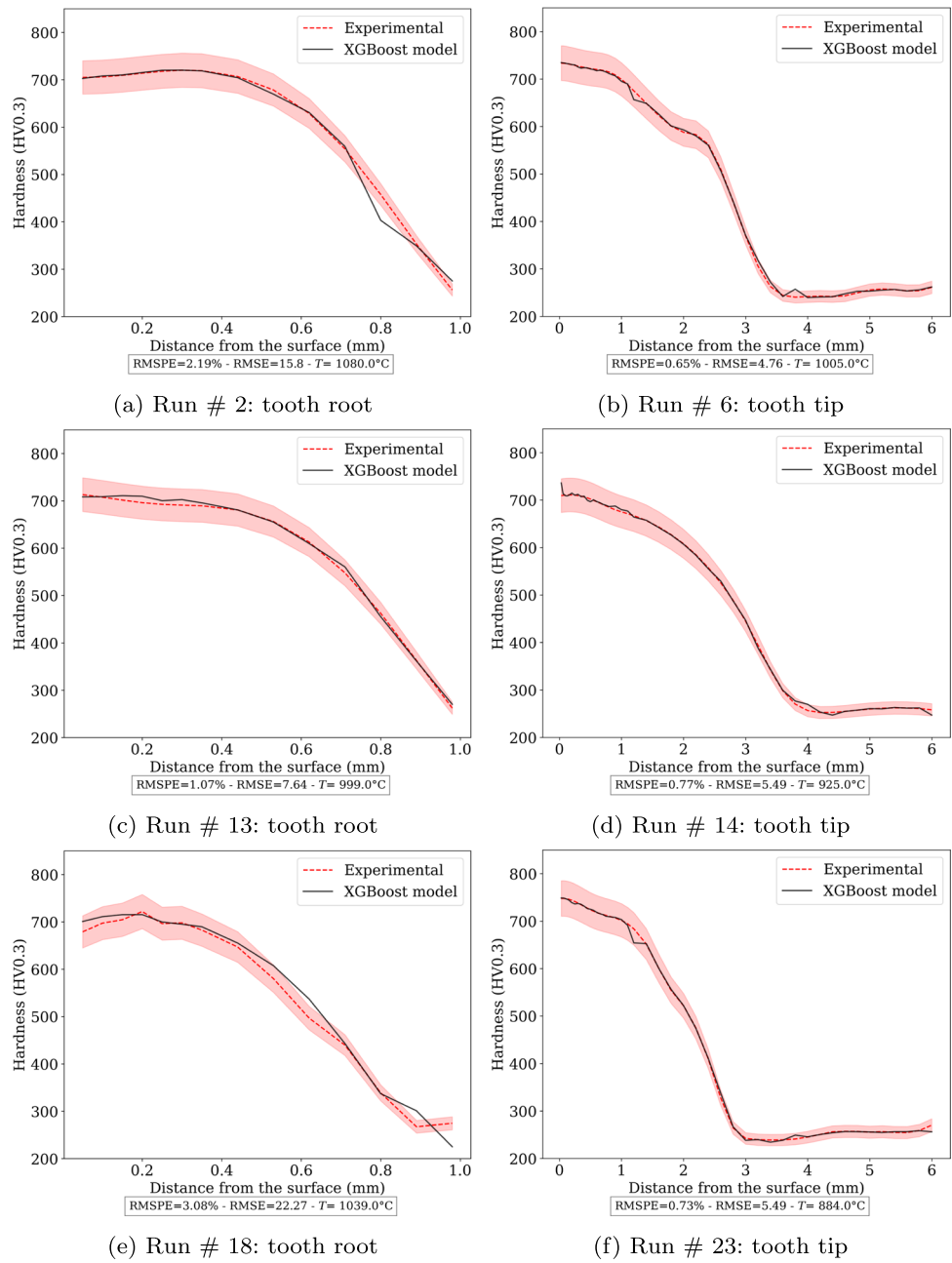


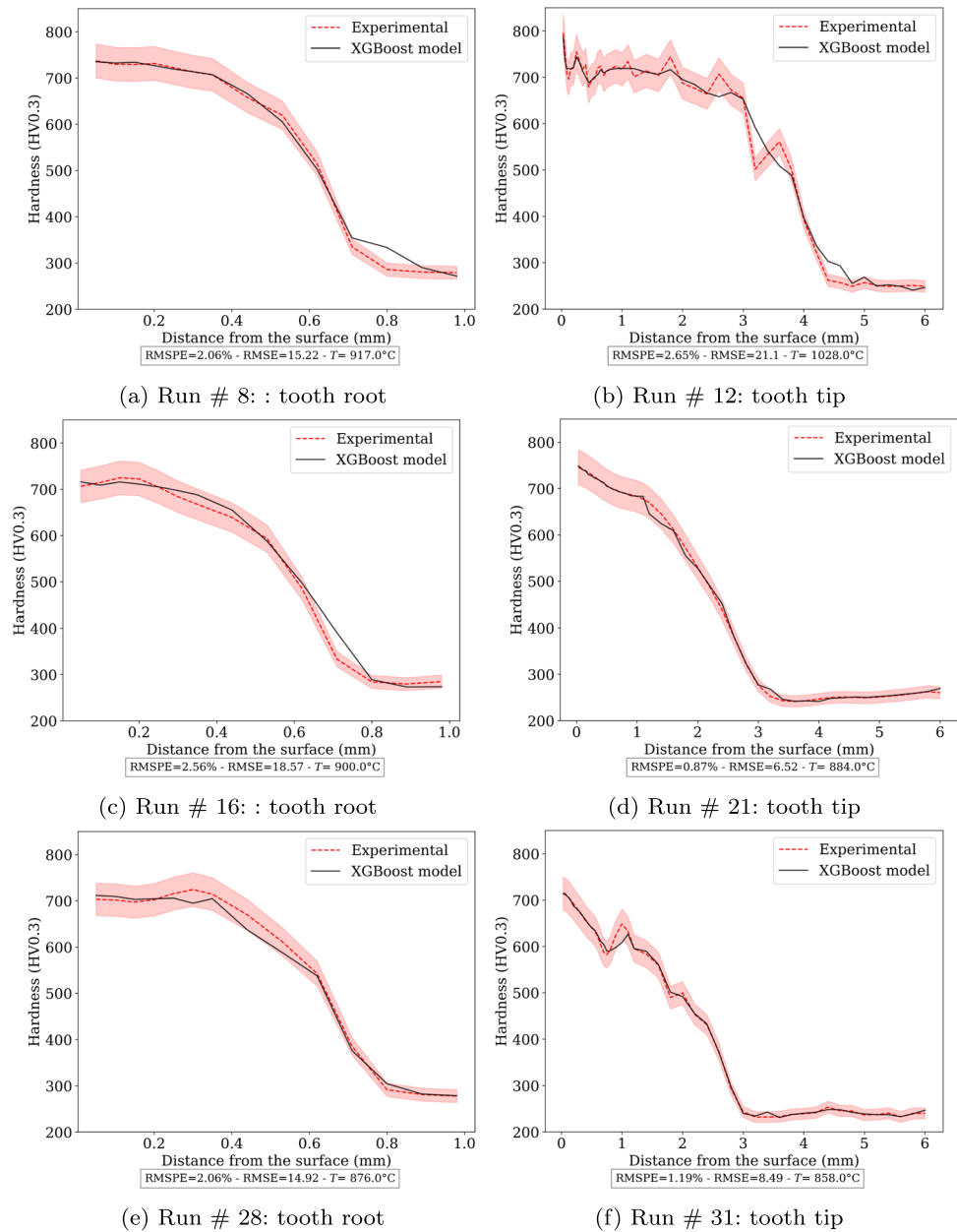
**Fig. 10** Comparison of the XGBoost model with the experimental hardness for the gear treated under double frequency - Case 2.  $T$  is the measured surface temperature



within 300M steel bar and C45 steel spur-gear. The capability of this approach to get a representative induction hardening treatment was evaluated and discussed. The main conclusions were as follows:

- Two experiments were carried out on cylinder bars and gears with single and double-frequency induction hardening, respectively. Data-driven models were developed based on XGBoost library, a tree-based gradient-boosted machine learning model.
- The low value of RMSPE and the accurate predicted profiles found indicated that the XGBoost model could adequately predict the hardness profiles.
- The space of variables did not have a significant impact on the training nor the testing results.
- Results showed that the XGBoost model predictions were in good agreement with experimental measurements in each case studied.

**Fig. 11** Comparison of the XGBoost model with the experimental hardness for the gear treated under double frequency - Case 3.  $T$  is the measured surface temperature



It is worth outlining that it is possible to improve the space of variables, considering in-depth temperature for the gear case and not only the surface temperature: it could be easier to describe the hardness. Even if the obtained results are satisfying, it is worth noticing that they can be improved with more runs considering more different process parameters. The predictions could be more accurate and provide a higher threshold of confidence. According to the obtained results, the proposed modeling can be used in induction treatment process optimization and extended to other geometries or treatments.

**Acknowledgements** This work was conducted with the help of the French Technological Research Institute for Materials, Metallurgy and

Processes (IRT-M2P). The authors would like to acknowledge IRTM2P and the partners of the project TRANSFUGE led by IRT-M2P.

## Declarations

**Conflicts of interest** The authors declare that they have no conflict of interest.

## Appendix A: XGBoost tree construction

Table 7 presents a simple matrix defined to be used with XGBoost algorithm.

**Fig. 12** Comparison of the XGBoost model with the experimental hardness for the gear treated under double frequency - Case 4.  $T$  is the measured surface temperature

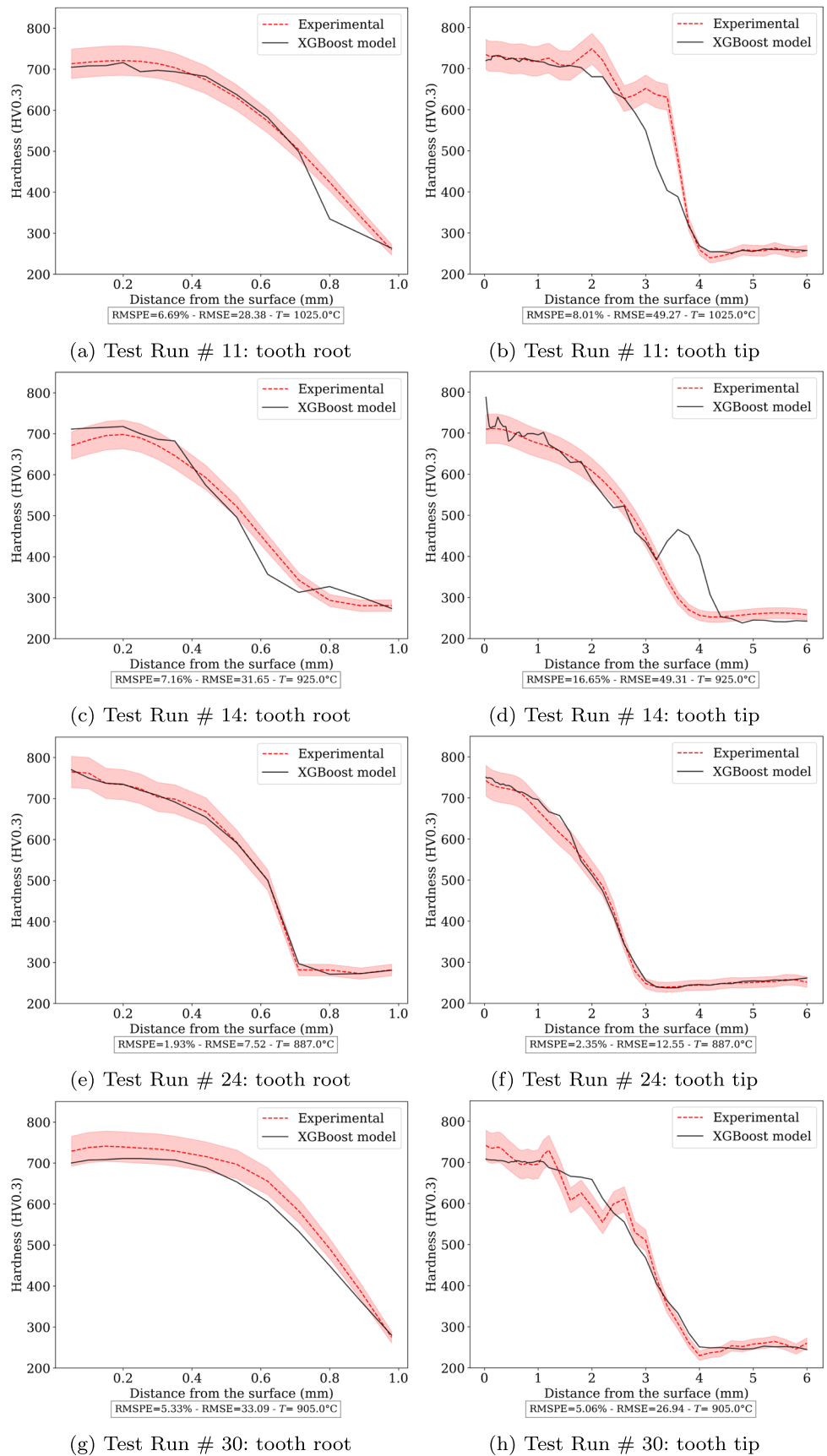


**Table 7** Example for XGBoost presentation

Index	Depth	Hardness
$k$	$d$ (mm)	$H$ (HV0.3)
1	0.1	700
2	2	300
3	3	700
4	5.5	600

**Residuals**

As mentioned, the first step is to get the initial prediction. If it is the first tree just like here, the value can be set as the mean of the hardness values. The first prediction  $y_{init}$  is then:

$$y_{init} = \frac{700 + 600 + 300 + 700}{4} = 575 \quad (13)$$

and the first residual should be  $r_1 = 700 - 575 = 125$  and all the residuals as illustrated in Fig. 13 for this first phase are:

$$r = \{125, 25, -275, 125\} \quad (14)$$

**Splitting**

Assume  $\lambda = 1$  for the example. The next step is to split the present node into two new nodes and go deeper in the it's time to split for new branches. As there are 4 values, there are 3 threshold for possible splits. All the different thresholds for the depth  $d$  are 1.05; 2.5; 4.25. The calculations are illustrated with there respective trees in Figs. 14, 15, 16.

Because the maximum gain  $G$  is obtained for the split with the threshold of  $d < 1.05$ , it is this one to be kept. Now, according to the maximum depth set in the hyperparameters, there are other splits to make. Because on the left branch there is one single residual left, the only next split should be on the right branch. The next calculations are done in the same way as presented for the split before.

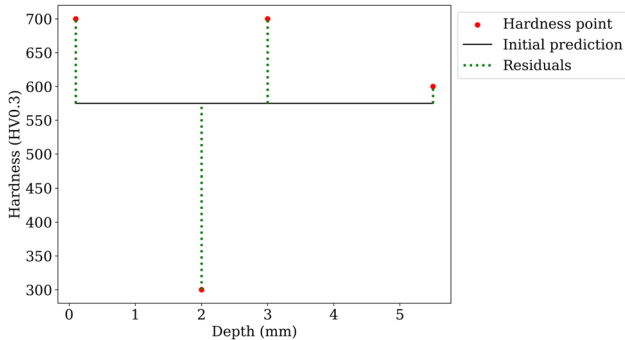


**Fig. 13** Residuals for the first tree

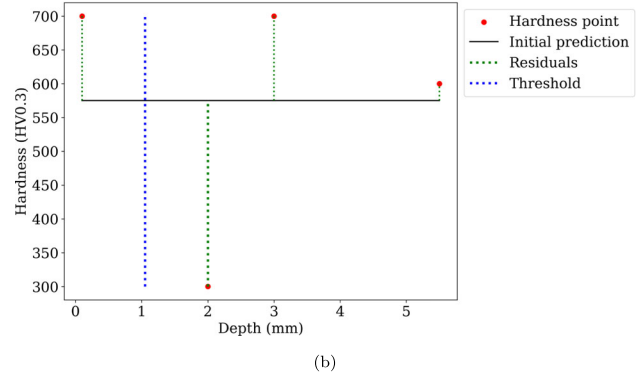
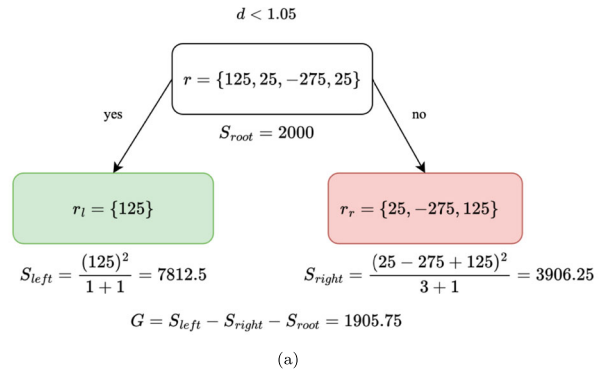


**Fig. 14** Split with the threshold  $d < 1.05$  and the respective tree

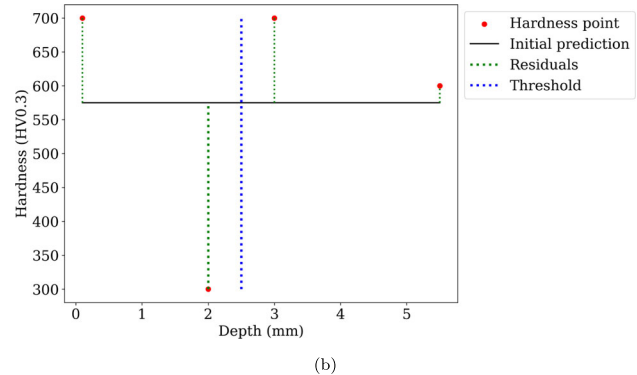
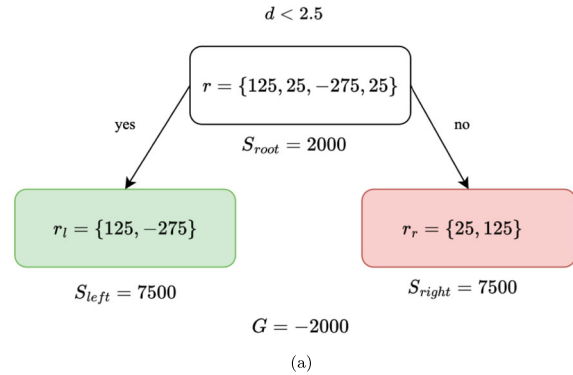


**Fig. 15** Split with the threshold  $d < 2.5$  and the respective tree

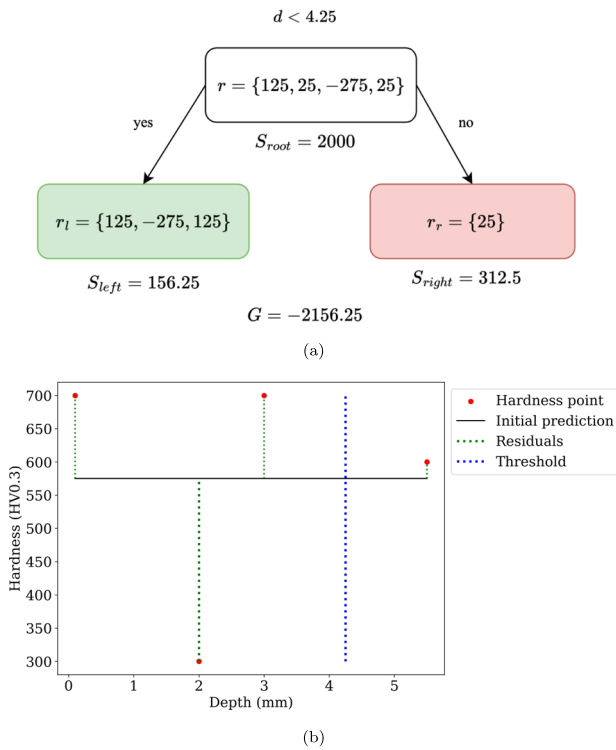


Fig. 16 Split with the threshold  $d < 4.25$  and the respective tree

### Output and predictions

When the tree is arrived at its final depth (here a depth of 3 for simplicity) and after tree optimization like pruning, the output must be calculated to get the tree predictions. The tree with the outputs is shown in Fig. 17.

With the outputs, it is now possible to calculate the predictions  $(\hat{y})_k$  of the hardness values with this first tree. The first value to predict, with a depth of  $d_1 = 0.1$ , has a tree output of  $Output = 62.5$  because  $d_1 < 1.05$ . Hence,

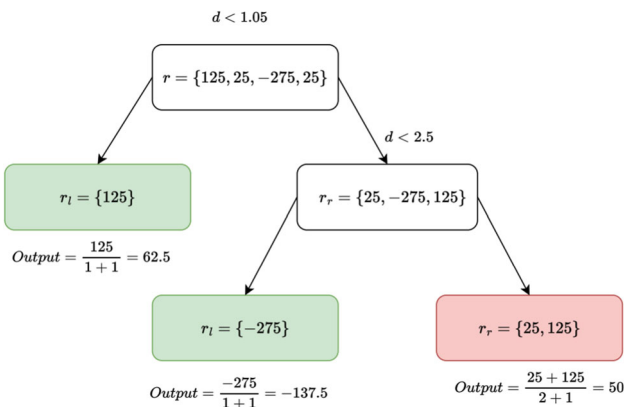


Fig. 17 Final tree with outputs

Table 8 Results of the first built tree

Index	Depth	Hardness	Predicted Hardness
$k$	$d$ (mm)	$H$ (HV0.3)	$\hat{y}$
1	0.1	700	593.5
2	2	300	533.5
3	3	700	590
4	5.5	600	590

Table 9 Residual difference between first tree and second tree

Index	First Residuals	New Residuals
$k$		
1	125	106.5
2	-275	-233.5
3	125	110
4	25	10

$\hat{y}_1 = y_{init} + \eta \times Output$  and the calculation is:

$$\hat{y}_1 = 575 + 0.3 \times 62.5 = 593.5$$

All the predicted values for this tree are listed in Table 8.

The next residuals must be now closer to 0 than the previous one, showing a better accuracy in prediction. The previous and new residuals are shown in Table 9. A new tree will be built on top of these latest predictions, to compute new residuals and build a better tree.

The trees must be built in this way sequentially until an hyperparameter or training condition is met.

### References

- Haimbaugh RE (2015) Practical induction heat treating. ASM international
- Qiu G, Zhan D, Li C, Yang Y, Qi M, Jiang Z, Zhang H (2020) Effects of yttrium and heat treatment on the microstructure and mechanical properties of clam steel. J Mater Eng Perform 29(1):42–52
- Celada-Casero C, Huang B, Yang J-R, San-Martin D (2019) Microstructural mechanisms controlling the mechanical behaviour of ultrafine grained martensite/austenite microstructures in a metastable stainless steel. Mater Des 181:107922
- Hömberg D, Liu Q, Montalvo-Urquizo J, Nadolski D, Petzold T, Schmidt A, Schulz A (2016) Simulation of multi-frequency-induction-hardening including phase transitions and mechanical effects. Finite Elem Anal Des 121:86–100
- Maresca F, Kouznetsova V, Geers M, Curtin W (2018) Contribution of austenite-martensite transformation to deformability of advanced high strength steels?: from atomistic mechanisms to microstructural response. Acta Mater 156:463–478
- Xu S, Li J, Cui Y, Zhang Y, Sun L, Li J, Luan J, Jiao Z, Wang X-L, Liu C et al (2020) Mechanical properties and deformation mechanisms of a novel austenite-martensite dual phase steel. Int J Plast 128:102677

7. Candeo A, Ducassy C, Bocher P, Dughiero F (2011) Multiphysics modeling of induction hardening of ring gears for the aerospace industry. *IEEE Trans Magn* 47(5):918–921
8. Wuppermann C, Míček E (2018) Importance of heat treatment for the variety of applications of modern materials. *Prozesswärme* 2018:95–101
9. Al Salkhadi AAM, (2021) Modélisation et simulation du procédé de durcissement par induction appliqué à des pignons à chaîne-chauffage à double fréquence. Ph.D. dissertation, Université du Québec à Rimouski
10. Barglik J, Ducki K, Kukla D, Mizera J, Mrówka-Nowotnik G, Sieniawski J, Smalcerz A (2018) Comparison of single and consecutive dual frequency induction surface hardening of gear wheels. In: *IOP conference series: materials science and engineering*, vol 355, IOP Publishing, pp 012015
11. Kristoffersen H, Vomacka P (2001) Influence of process parameters for induction hardening on residual stresses. *Mater Des* 22(8):637–644. <https://linkinghub.elsevier.com/retrieve/pii/S0261306901000334>
12. Li J, Cao Z, Liu L, Liu X, Peng J (2021) Effect of microstructure on hardness and wear properties of 45 steel after induction hardening. *Steel Res Int* 92(4):2000540. <https://onlinelibrary.wiley.com/doi/10.1002/srin.202000540>
13. Hájek J, Rot D, Jiřinec J (2019) Distortion in induction-hardened cylindrical part. *Defect Diff Forum* 395:30–44. <https://www.scientific.net/DDF.395.30>
14. Grum J (2001) A review of the influence of grinding conditions on resulting residual stresses after induction surface hardening and grinding. *J Mater Process Technol* p 15
15. Rodman D, Krause C, Nürnberger F, Bach F-W, Haskamp K, Kästner M, Reithmeier E (2011) Induction hardening of spur gearwheels made from 42CrMo4 hardening and tempering steel by employing spray cooling. *Steel Res Int* 82(4):329–336 <https://onlinelibrary.wiley.com/doi/10.1002/srin.201000218>
16. Yi J, Gharghoury M, Bocher P, Medraj M (2013) Distortion and residual stress measurements of induction hardened AISI 4340 discs. *Mater Chem Phys* 142(1):248–258. <https://linkinghub.elsevier.com/retrieve/pii/S025405841300535X>
17. Hutton DV (2003) *Fundamentals of finite element analysis*. McGraw-Hill Science Engineering
18. Guo Y, Liu M, Yan Y (2021) Hardness prediction of grind-hardening layer based on integrated approach of finite element and cellular automata. *Materials* 14(19):5651
19. Derouiche K, Garois S, Champaney V, Daoud M, Traidi K, Chinesta F (2021) Data-driven modeling for multiphysics parametrized problems-application to induction hardening process. *Metals* 11(5):738
20. Zhang Y, Ruan J, Huang T, Yang X, Zhu H, Yang G (2012) Calculation of temperature rise in air-cooled induction motors through 3-d coupled electromagnetic fluid-dynamical and thermal finite-element analysis. *IEEE Trans Magn* 48(2):1047–1050
21. Javaheri V, Pohjonen A, Asperheim JI, Ivanov D, Porter D (2019) Physically based modeling, characterization and design of an induction hardening process for a new slurry pipeline steel. *Mater Des* 182:108047
22. Daoud M, Kubler R, Bemou A, Osmond P, Polette A (2021) Prediction of residual stress fields after shot-peening of trip780 steel with second-order and artificial neural network models based on multi-impact finite element simulations. *Journal of Manufacturing Processes* 72:529–543
23. Fisk M, Lindgren L-E, Datchary W, Deshmukh V (2018) Modelling of induction hardening in low alloy steels. *Finite elements in analysis and design* 144:61–75
24. Sumithra P, Thiripurasundari D (2017) Review on computational electromagnetics. *Advanced Electromagnetics* 6(1):42–55
25. W. Li, Z Yuan, and Z Chen (2013) Adaptive mesh morphing method for numerical analysis of electromagneto-mechanical coupling using lagrangian approach. In: *Proc 19th Int Conf Comput Electromagn Fields COMPUMAG*, pp 1–2
26. N. Barka, P Bocher, J Brousseau, M Galopin, and S Sundararajan (2007) Modeling and sensitivity study of the induction hardening process. In: *Advanced Materials Research*, vol 15. Trans Tech Publ, pp 525–530
27. Leitner M, Aigner R, Grün F (2019) Numerical fatigue analysis of induction-hardened and mechanically post-treated steel components. *Machines* 7(1):1
28. Kurek K, Dolega D (2003) Modeling of induction hardening. *Int sci colloquium?: modeling of electromagnetic processing*. Hannover, Germany, pp 125–130
29. Kennedy MW, Akhtar S, Bakken JA, Aune RE (2011) Analytical and experimental validation of electromagnetic simulations using comsol®, reinductance, induction heating and magnetic fields. *COMSOL users conference*. Stuttgart Germany, Citeseer, pp 1–9
30. M. W. Kennedy, S Akhtar, JA Bakken, and RE Aune (2011) Review of classical design methods as applied to aluminum billet heating with induction coils. In: *EPD congress 2011-TMS 2011 annual meeting and exhibition*; San Diego, CA, United States, 27 February-3 March, 2011, pp 707–722
31. Areitioaurtena M, Segurajauregi U, Akujärvi V, Fisk M, Urresti I, Ukar E (2021) A semi-analytical coupled simulation approach for induction heating. *Advanced Modeling and Simulation in Engineering Sciences* 8(1):1–19
32. Hömberg D, Petzold T, Rocca E (2015) Analysis and simulations of multifrequency induction hardening. *Nonlinear Analysis: Real World Applications* 22:84–97
33. Smokvina Hanza S, Marohnić T, Iljkić D, Basan R (2021) Artificial neural networks-based prediction of hardness of low-alloy steels using specific jominy distance. *Metals* 11(5):714
34. Asadzadeh MZ, Raninger P, Prevedel P, Ecker W, Mücke M (2021) Hybrid modeling of induction hardening processes. *Applications in Engineering Science* 5:100030
35. A. Sorsa, K Leiviskä, S Santa-aho, and T Lepistö (2012) Quantitative prediction of residual stress and hardness in case-hardened steel based on the Barkhausen noise measurement. *NDT E International* 46:100–106. <https://linkinghub.elsevier.com/retrieve/pii/S0963869511001733>
36. J. Wróbel and A. Kulawik (2015) Using the artificial neural networks in the modelling of the induction heating. In: *AIP conference proceedings*, vol 1648. AIP Publishing LLC, pp 850090
37. P. D. Deshpande, B. Gautham, U. Gupta, and D. Khan (2014) Modeling the steel case carburizing quenching process using statistical and machine learning techniques. In: *2014 9th international conference on industrial and information systems (ICIIS)*, IEEE, pp 1–6
38. Lambiase F, Di Ilio A, Paoletti A (2013) Prediction of laser hardening by means of neural network. *Procedia CIRP* 12:181–186
39. Ghaisari J, Jannesari H, Vatani M (2012) Artificial neural network predictors for mechanical properties of cold rolling products. *Advances in Engineering Software* 45(1):91–99
40. T. Chen and C. Guestrin (2016) Xgboost: a scalable tree boosting system. [arXiv:1603.02754](https://arxiv.org/abs/1603.02754)
41. L. Ruisen, D. Songyi, W. Chen, C. Peng, T. Zuodong, Y. YanMei, and W. Shixiong (2018) Bagging of xgboost classifiers with random under-sampling and totem link for noisy label-imbalanced data. In: *IOP conference series: materials science and engineering*, vol 428. IOP Publishing, pp 012004
42. Nenchev B, Tao Q, Dong Z, Panwisawas C, Li H, Tao B, Dong H (2022) Evaluating data-driven algorithms for predicting mechanical properties with small datasets: a case study on gear steel hardenability. *Int J Miner Metall Mater* 29(4):836–847

- 
43. Chen J, Zhao F, Sun Y, Zhang L, Yin Y (2019) Prediction model based on xgboost for mechanical properties of steel materials. *International Journal of Modelling, Identification and Control* 33(4):322–330
  44. Schwenk M, Fisk M, Cedell T, Hoffmeister J, Schulze V, Lindgren L-E (2012) Process simulation of single and dual frequency induction surface hardening considering magnetic nonlinearity. *Materials Performance and Characterization* 1(1):1–20
  45. Schwenk M, Hoffmeister J, Schulze V (2014) Experimentally validated residual stresses and distortion prediction for dual frequency induction hardening. *International Journal of Applied Electromagnetics and Mechanics* 44(2):127–135
  46. Yun D, Park H, Koo J-H, Ham S, Lee S (2015) Investigation of heat treatment of gears using a simultaneous dual frequency induction heating method. *IEEE Transactions on Magnetics* 51(11):1–4
  47. Iso E (2018) 6507–1: 2018-metallic materials-vickers hardness test-part 1: test method. Geneva, Switzerland, ISO
  48. Tamayo D, Silburt A, Valencia D, Menou K, Ali-Dib M, Petrovich C, Huang CX, Rein H, Van Laerhoven C, Paradise A et al (2016) A machine learns to predict the stability of tightly packed planetary systems. *The Astrophysical Journal Letters* 832(2):L22
  49. Möller A, Ruhlmann-Kleider V, Leloup C, Neveu J, Palanque-Delabrouille N, Rich J, Carlberg R, Lidman C, Pritchett C (2016) Photometric classification of type Ia supernovae in the supernova legacy survey with supervised learning. *Journal of Cosmology and Astroparticle Physics* 2016(12):008
  50. F. Giannakas, C. Troussas, A. Krouska, C. Sgouropoulou, and I. Voyiatzis (2021) Xgboost and deep neural network comparison: The case of teams' performance. In: *International conference on intelligent tutoring systems*, Springer, pp 343–349
  51. Zamani JM, Cao C, Ni X, Bashir B, Talebiesfandarani S (2019) Pm2. 5 prediction based on random forest, xgboost, and deep learning using multisource remote sensing data. *Atmosphere* 10(7):373
  52. T. S. Jaakkola and D. Haussler (1999) Probabilistic kernel regression models. In: *Seventh international workshop on artificial intelligence and statistics*, PMLR

**Publisher's Note** Springer Nature remains neutral with regard to jurisdictional claims in published maps and institutional affiliations.

Springer Nature or its licensor (e.g. a society or other partner) holds exclusive rights to this article under a publishing agreement with the author(s) or other rightsholder(s); author self-archiving of the accepted manuscript version of this article is solely governed by the terms of such publishing agreement and applicable law.